

Electronic Supplementary Information (ESI)

**Hydrogen bonded organic framework pores differentially
loading triazole for photocatalytic uranium reduction**

Qiong Wu,^{a, ‡} Ying-Ao Wang,^{a, ‡} Xun Wang,^a Qiao-Qiao Jiang,^a Ya-Jie Li,^a Ru-Ping
Liang,^{a*} Jian-Ding Qiu^{a,b*}

^a School of Chemistry and Chemical Engineering, Nanchang University, Nanchang
330031, China

^b National Key Laboratory of Uranium Resources Exploration-Mining and Nuclear
Remote Sensing, East China University of Technology, Nanchang 330013, China

[‡]These authors contributed equally.

*Corresponding authors. Tel/Fax: +86-791-83969518. E-mail: rpliang@ncu.edu.cn; jdqiu@ncu.edu.cn

Table of contents

1. Supplementary Notes.....	S3
2. Supplementary Methods.....	S4
2.1 Synthesis of HOF-C and HOF-K.....	S4
2.2 Synthesis of HOF-C-TRZ and HOF-K/TRZ.....	S4
2.3 Uranium photocatalytic removal isotherms.....	S4
2.4 Uranium removal kinetics.....	S5
2.5 Selectivity test.....	S5
2.6 Recyclability test.....	S6
2.7 Theoretical calculations.....	S6
3. Supplementary Figures and Tables.....	S7
4. Supplementary References.....	S21

1. Supplementary Notes.

Tris(4-(4H-1,2,4-triazol-4-yl)phenyl)amine (TTPA) was purchased from Jilin Chinese Academy of Sciences-Yanshen Technology Co., Ltd., without further purification. Nitric acid, ethyl alcohol and N, N-dimethylformamide were purchased from Sinopharm Chemical Reagent Co., Ltd. Ultrapure water was made by the Millipore system ($18.25 \text{ M}\Omega \text{ cm}^{-1}$).

X-ray diffraction (XRD) data of the nanomaterial were collected on a Bruker AXS D8 Advance A25 Powder X-ray diffractometer (40 kV, 40 mA) using Cu $K\alpha$ ($\lambda=1.5406 \text{ \AA}$) radiation. The ultraviolet-visible diffuse reflectance spectra (UV-vis DRS) were recorded at room temperature on a HITACHI U-4100 Spectrophotometer. Photocurrent responses, cyclic voltammetry (CV), Mott-Schottky (M-S) and electrochemical impedance spectroscopy (EIS) were recorded on CHI660 electrochemical workstation in a classical three-electrode configuration consisting of a modified working electrode, a platinum counter electrode and an Ag/AgCl reference electrode. The morphology of the cocrystals were collected on a scanning electron microscope (SEM, JEM-2010, JEOL). X-ray photoelectron spectroscopy (XPS) spectra were performed on a Thermo VG Multilab 2000X with Al $K\alpha$ irradiation. The nitrogen adsorption and desorption isotherms were measured at 77 K using a Micromeritics ASAP 2020M system. The samples were outgassed at 120 °C for 8 h before the measurements. Surface areas were calculated from the adsorption data using Brunauer-Emmett-Teller (BET) method. The pore-size-distribution curves were obtained via the non-local density functional theory (NLDFT) method. Metal ions concentrations were determined using an iCAP Q inductively coupled plasma mass spectrometry (ICP-MS, Thermo Fisher Scientific, USA). Steady-state photoluminescence (PL) emission spectra and PL decay spectra were measured at room temperature using FLS 1000 spectrometer (Edinburgh Instruments, UK). The photocurrent responses were conducted with a CHI 660B workstation. The light was generated by a 300 W xenon lamp (PLS-SXE300D) with a light density of 1 kW m^{-2} at room temperature with the light wavelength from 300 nm to 2500 nm. Hydrogen bonded organic frameworks (HOFs) was mounted on loop for the X-ray measurement.

Diffraction data were collected on SuperNova (Dual source) diffractometer equipped with graphic monochromatic Cu K α radiation ($\lambda = 1.54184 \text{ \AA}$) using the CrysAlispro X-ray crystallography data systems at 100 K under a cold nitrogen stream. The structure of the materials was solved with the ShelXT structure solution program adopting Intrinsic Phasing and refined with the ShelXL refinement package adopting Least Squares minimisation by Olex2.^{1,2} The crystal data of HOF-C and HOF-K are listed in Table S1 and S2.

2. Supplementary Methods.

2.1 Synthesis of HOF-C and HOF-K.

Using tris(4-(4H-1,2,4-triazol-4-yl)phenyl)amine (TTPA) (44.6 mg) as reaction material, added with dilute nitric acid (60 μL), ethyl alcohol (1 mL), ultrapure (1 mL), 1 mL) and N, N-dimethylformamide (1 mL), and then sonicated to obtain the reaction mixture. The reaction mixture was heated to 90 $^{\circ}\text{C}$ at 5 $^{\circ}\text{C min}^{-1}$ for 3 days by solvothermal method, and then cooled to 40 $^{\circ}\text{C}$ or 30 $^{\circ}\text{C}$ within 24 h. The cluster and block crystals were collected separately. The cluster hydrogen bonded organic framework (HOF-C) and the block hydrogen bonded organic framework (HOF-K) were obtained after washing and drying.

2.2 Synthesis of HOF-C-TRZ and HOF-K/TRZ.

The HOF-C and HOF-K were sonicated at 1:4 with the guest triazole (TRZ) for 2 h to obtain the cluster HOF-C-TRZ inserted with TRZ and the block HOF-K/TRZ without TRZ insertion.

2.3 Uranium photocatalytic removal isotherms.

Considering that uranium exists mainly in the strong acidic environment and hydrolysis occurs in higher pH value, photoreduction experiments were carried out at pH 5.0. The catalyst (5 mg) was added to a 20 mL aqueous solution (contains 0.1 mL of methanol) with different concentrations of UO_2^{2+} (10, 50, 100, 150, 200, 300, 400 and 500 mg L^{-1}). After ultrasound treatment in the dark for 10 min, the adsorption and desorption equilibrium was achieved by standing treatment for 2 h. Finally, it was placed under Xe light source and irradiated for 3 h. The treated solution was filtered through a 0.22 μm membrane filter, and the filtrate was analyzed by ICP-MS to

determine the remaining UO_2^{2+} concentration. The removal capacity (q_e , mg g^{-1}) at equilibrium is calculated by $q_e = (C_0 - C_e)/m \times V$, where V (L) is the volume of the treated solution, m (g) is the amount of used catalyst, and C_0 and C_e (mg L^{-1}) are the initial concentration and the final equilibrium concentration of UO_2^{2+} , respectively. The experimental data were fitted by the Langmuir isotherm model. It can be described as: $q_e = q_m b C_e / (1 + b C_e)$, where b (L mg^{-1}) represents the Langmuir constant, C_e (mg L^{-1}) represents the equilibrium concentration of metal ions, q_m (mg g^{-1}) represents the monolayer adsorption capacity, q_e (mg g^{-1}) represent the equilibrium removal capacity.^{3,4}

2.4 Uranium removal kinetics.

The catalyst (5 mg) was added to an Erlenmeyer flask containing UO_2^{2+} solution (20 mL, contains 0.1 mL of methanol) at 500 mg L^{-1} and pH 5.0. The catalyst was completely suspended by sonication for 10 min in the dark, the adsorption and desorption equilibrium was achieved by standing treatment for 2 h. Finally, the mixture was vigorously stirred for different times under the light. The treated solution was filtered through a $0.22 \mu\text{m}$ membrane filter, and the filtrate was collected and analyzed by ICP-MS to determine the remaining UO_2^{2+} content. The experimental data was fitted using Pseudo-second-order kinetic model. It can be expressed as follows: $t/q_t = 1/(k_2 q_e^2) + t/q_e$, where q_t and q_e (mg g^{-1}) represent the removal amount at time and at equilibrium t (min), respectively, k_2 ($\text{g mg}^{-1} \text{ min}^{-1}$) represents the Pseudo-second-order rate constant of adsorption. The percentage removal of uranium concentration was calculated as follows: $R\% = (C_0 - C_e)/C_0 \times 100\%$, C_0 and C_e (mg L^{-1}) are the initial concentration and the final equilibrium concentration of UO_2^{2+} , respectively.⁵

2.5 Selectivity test.

The ions stock solutions (500 mg g^{-1}) were prepared by dissolving the corresponding nitrate salts or sodium salts of Mg^{2+} , Cu^{2+} , Zn^{2+} , Na^+ , K^+ , Pb^{2+} , Ca^{2+} , Fe^{3+} , Cr^{3+} , Eu^{3+} , VO_4^{3-} , Cd^{2+} and UO_2^{2+} in ultrapure water. The concentration ratio of UO_2^{2+} (100 mg L^{-1}) and other ions was prepared at 1:5 to carry out the adsorption experiment. The removal capacity (q , mg g^{-1}) was calculated by $q = (C_0 - C_e)/m \times V$,

where V (L) is the volume of the treated solution, m (g) is the amount of used catalyst, and C_0 and C_e (mg L^{-1}) are the initial concentration and the final equilibrium concentration of different ions, respectively.

2.6 Recyclability test.

After catalysis, HOF-C-TRZ was centrifuged, eluted with 0.1 M HNO_3 aqueous solution, and washed with ultra-pure water many times until it became neutral. HOF-C-TRZ was dried under vacuum then photocatalytic experiment was carried out.

2.7 Theoretical calculations.

The equilibrium morphologies of HOFs were simulated by Materials Studio and Diamond software. The density functional theory (DFT) calculations were carried out in Gaussian 09 program calculated by the B3LYP functional and 6-311G (d) basis set. Grimme's D3BJ dispersion correction was used to improve calculation accuracy. The calculation object of Van der Waals surface electrostatic potential (ESP) is partial structure with optimized ground state geometry. The ESP analysis is performed by Multiwfn package and the graphs of which were rendered by VMD. The calculation object of binding energy is partial structure with optimized ground state geometry. The binding energy analysis and image generation were performed by Gaussian 09 program.

3. Supplementary Figures and Tables.

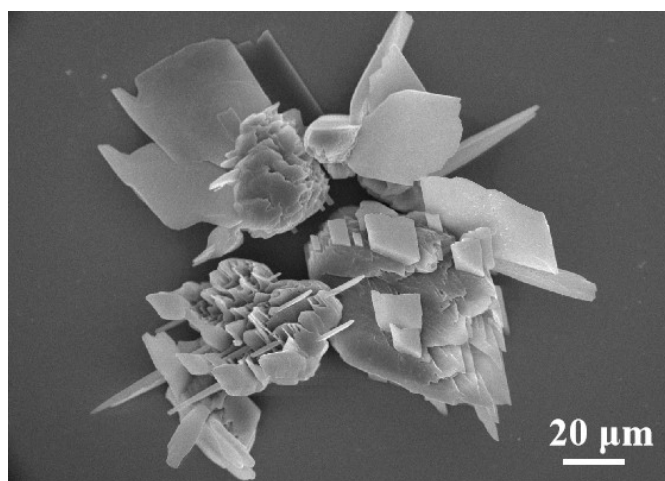


Fig. S1. SEM images of cococrystals HOF-C.

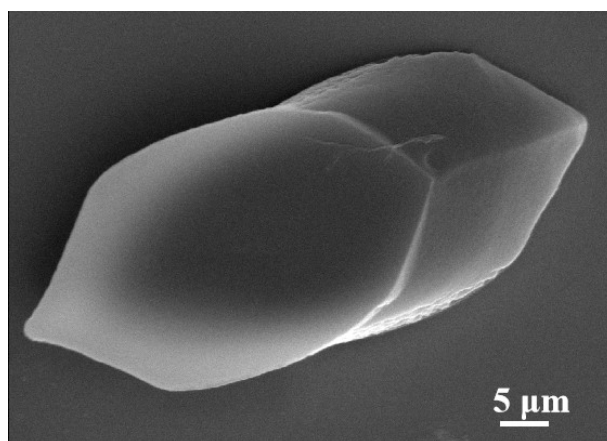


Fig. S2. SEM images of cococrystals HOF-K.

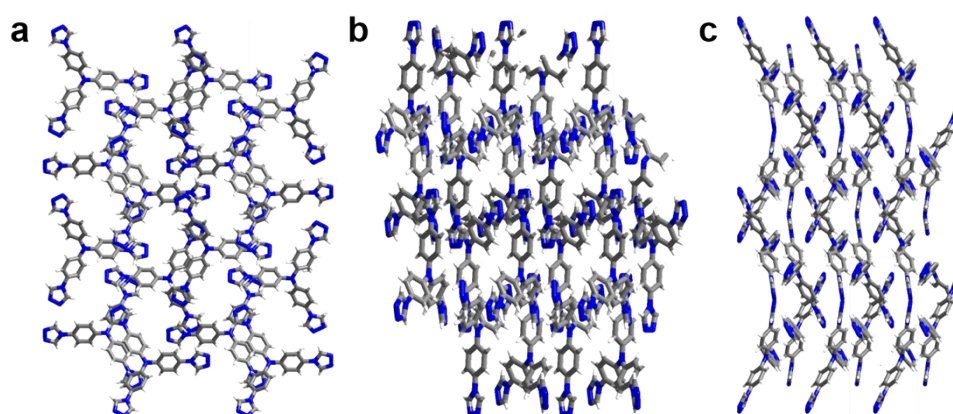


Fig. S3. (a) a-axis packing structures of HOF-C. (b) b-axis packing structures of HOF-C. (c) c-axis packing structures of HOF-C. Gray, white and blue balls denote C, H and N atoms, respectively.

Table S1. Single-crystal X-ray structure refinement of HOF-C.

Identification code	HOF-C
CCDC	2361481
Empirical formula	C ₂₄ H ₁₈ N ₁₀
Formula weight	446.48
Temperature/K	293(2)
Crystal system	monoclinic
Space group	P2 ₁ /c
a/Å	8.42054(13)
b/Å	20.9619(2)
c/Å	15.44455(16)
α /°	90
β /°	96.1582(11)
γ /°	90
Volume/Å ³	2710.39(6)
Z	4
$\rho_{\text{calc}}/\text{cm}^3$	1.094
μ/mm^{-1}	0.575
F(000)	928.0
Radiation	Cu K α ($\lambda = 1.54184$)
2 Θ range for data collection/°	7.136 to 150.32
Index ranges	-9 \leq h \leq 10, -26 \leq k \leq 26, -19 \leq l \leq 19
Reflections collected	63978
Independent reflections	5465 [$R_{\text{int}} = 0.0496$, $R_{\text{sigma}} = 0.0223$]
Data/restraints/parameters	5465/0/307
Goodness-of-fit on F ²	2.636
Final R indexes [$I \geq 2\sigma(I)$]	$R_1 = 0.0801$, $wR_2 = 0.3126$
Final R indexes [all data]	$R_1 = 0.0877$, $wR_2 = 0.3196$
Largest diff. peak/hole / e Å ⁻³	0.47/-0.25

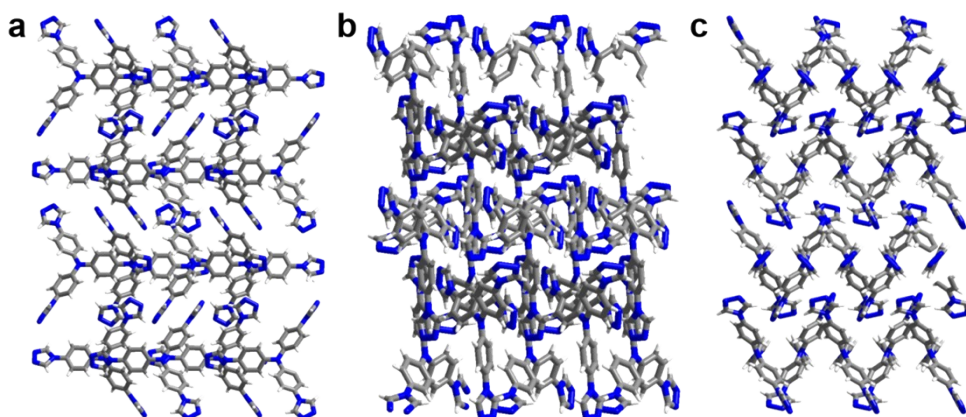


Fig. S4. (a) a-axis packing structures of HOF-K. (b) b-axis packing structures of HOF-K. (c) c-axis packing structures of HOF-K. Gray, white and blue balls denote C, H and N atoms, respectively.

Table S2. Single-crystal X-ray structure refinement of HOF-K.

Identification code	HOF-K
CCDC	2361483
Empirical formula	$C_{24}H_{18}N_{10}$
Formula weight	446.48
Temperature/K	293(2)
Crystal system	monoclinic
Space group	$P2_1/n$
$a/\text{\AA}$	8.2639(3)
$b/\text{\AA}$	20.5086(8)
$c/\text{\AA}$	12.6508(5)
$\alpha/^\circ$	90
$\beta/^\circ$	93.880(3)
$\gamma/^\circ$	90
Volume/ \AA^3	2139.16(14)
Z	4
$\rho_{\text{calc}}/\text{g/cm}^3$	1.386

μ/mm^{-1}	0.729
F(000)	928.0
Radiation	CuK α ($\lambda = 1.54184$)
2θ range for data collection/ $^\circ$	8.226 to 149.868
Index ranges	$-10 \leq h \leq 10, -24 \leq k \leq 25, -15 \leq l \leq 14$
Reflections collected	14321
Independent reflections	4212 [$R_{\text{int}} = 0.0253, R_{\text{sigma}} = 0.0235$]
Data/restraints/parameters	4212/0/308
Goodness-of-fit on F^2	1.055
Final R indexes [$I \geq 2\sigma(I)$]	$R_1 = 0.0460, wR_2 = 0.1304$
Final R indexes [all data]	$R_1 = 0.0516, wR_2 = 0.1357$
Largest diff. peak/hole / $e \text{ \AA}^{-3}$	0.72/-0.21

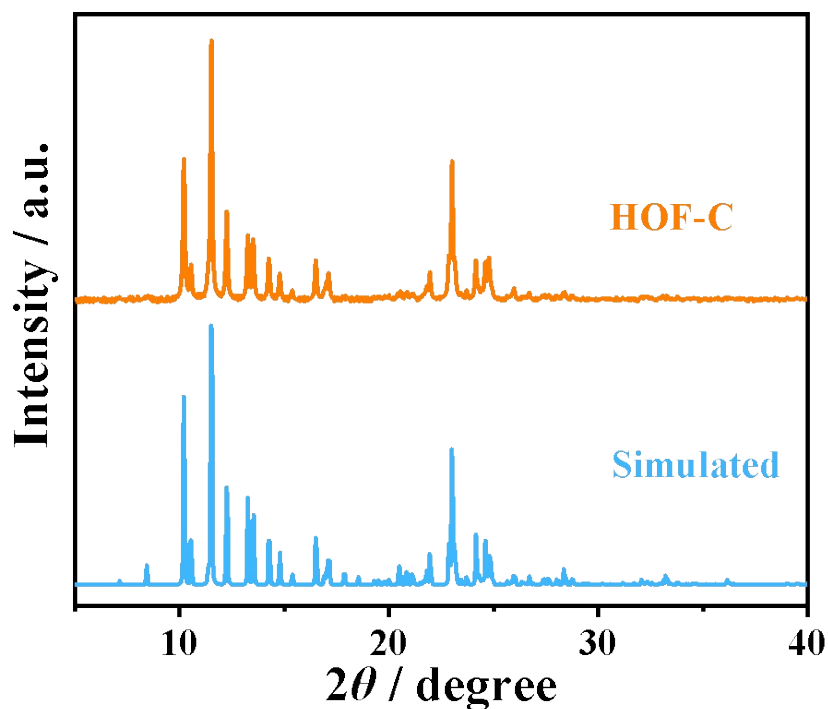


Fig. S5. The XRD patterns of HOF-C: the experimental result (orange line), the simulated stacking mode result (blue line).

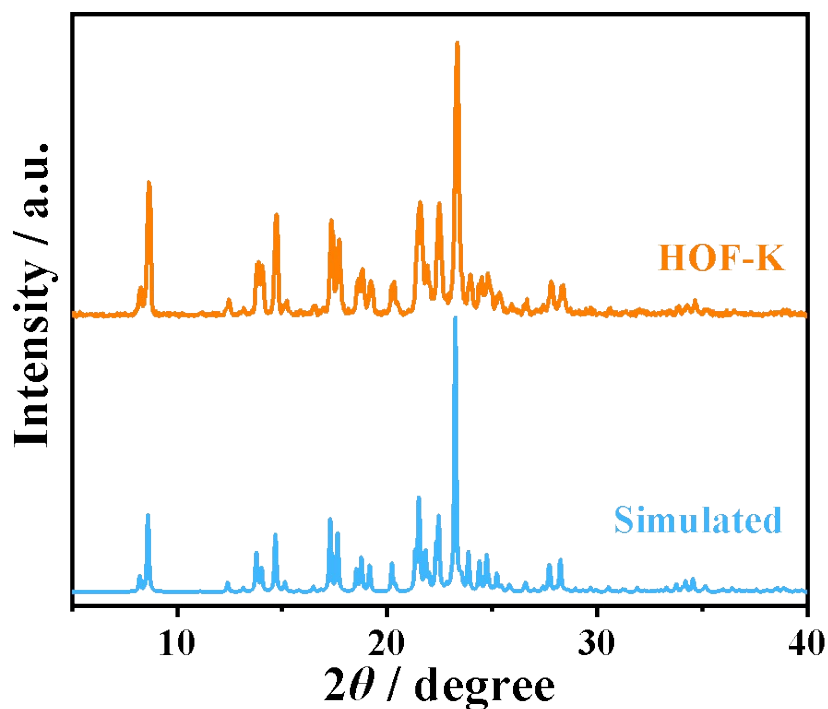


Fig. S6. The XRD patterns of HOF-K: the experimental result (origin line), the simulated stacking mode result (blue line).

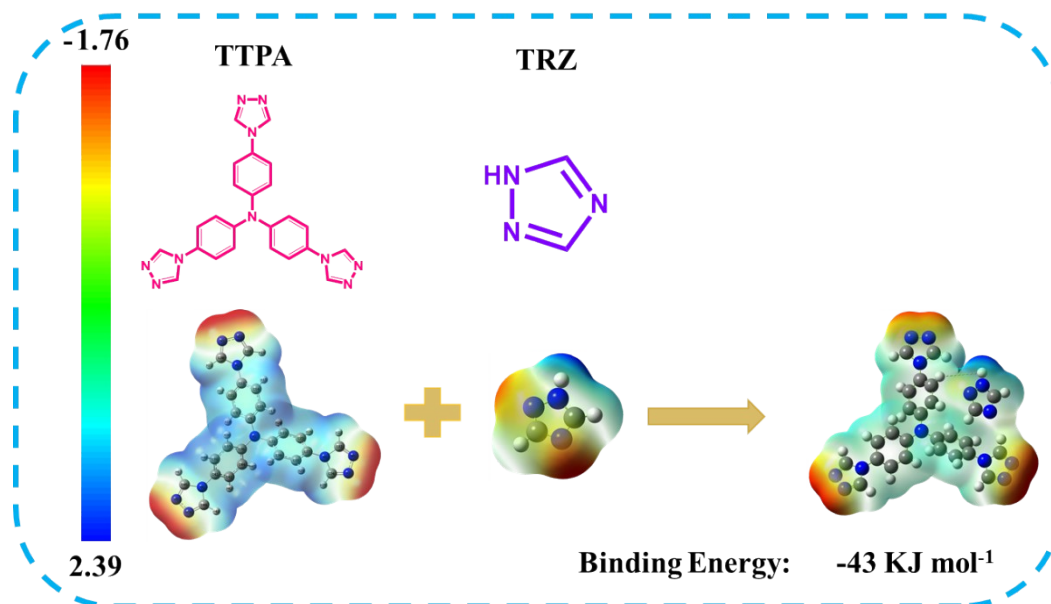


Fig. S7. Electrostatic surface potential analysis of TTPA, TRZ and the binding energy of TTPA with TRZ. (Red represents a rich charge and is electronegative. Blue means lack of charge, positive electricity).

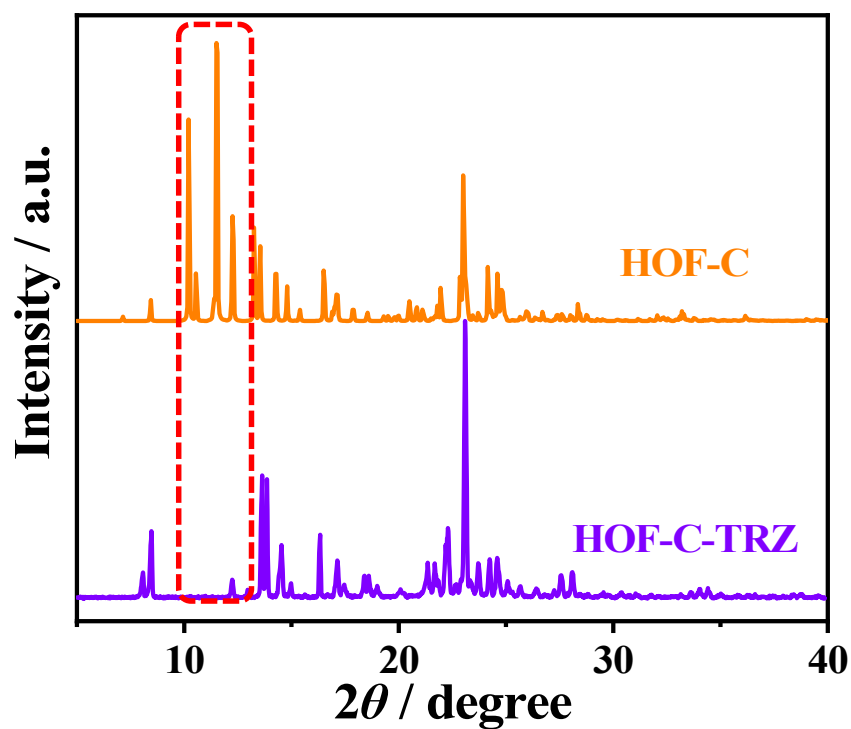


Fig. S8. The XRD patterns of HOF-C and HOF-C-TRZ.

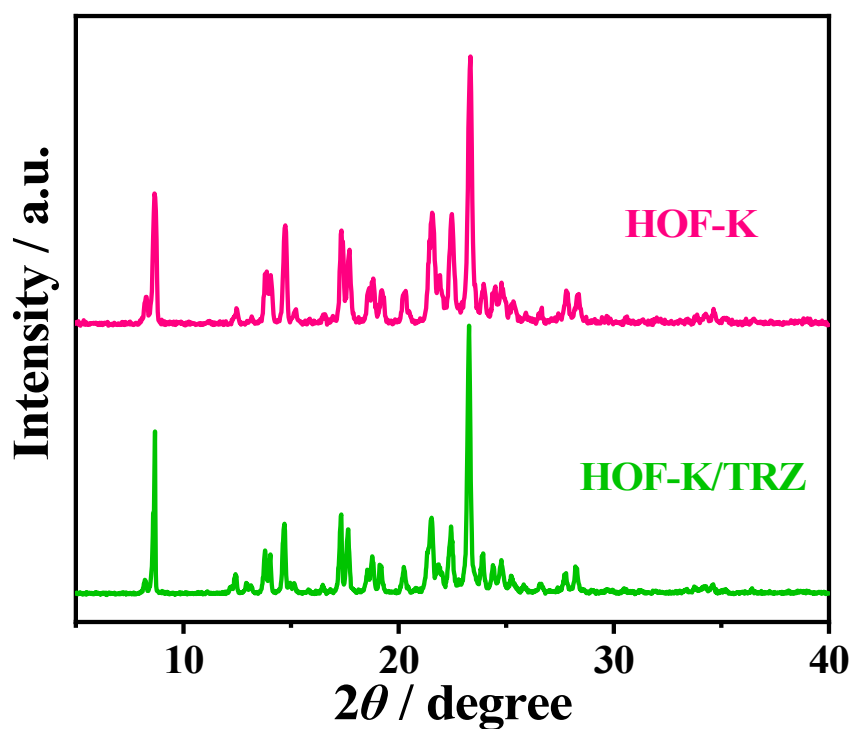


Fig. S9. The XRD patterns of HOF-K and HOF-K/TRZ.

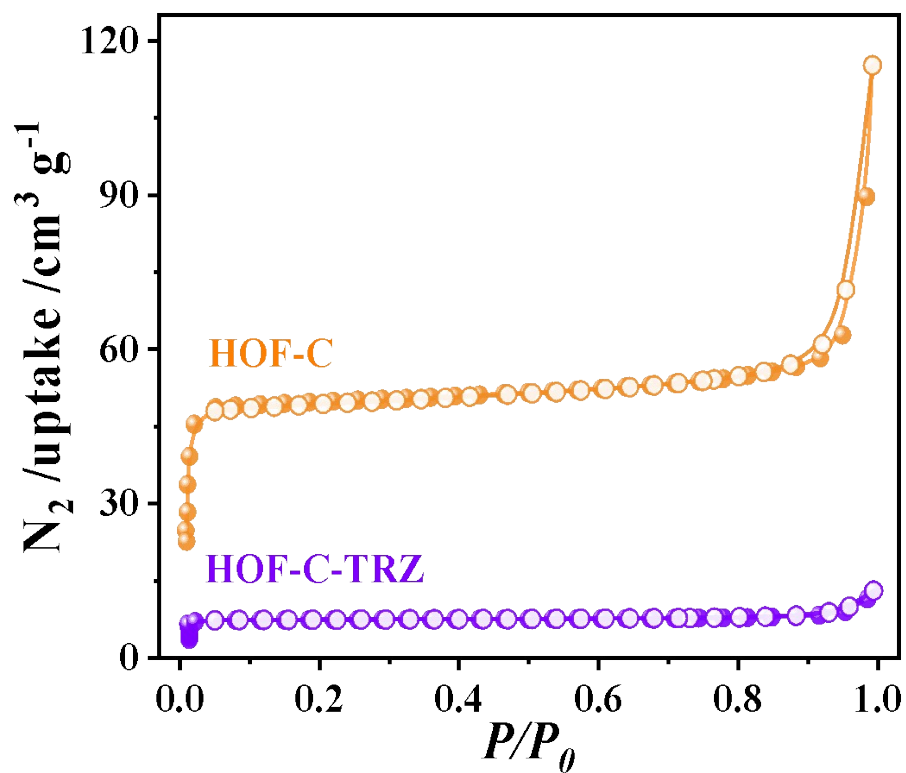


Fig. S10. The N_2 adsorption-desorption isotherm of HOF-C (orange line) and HOF-C-TRZ (purple line).

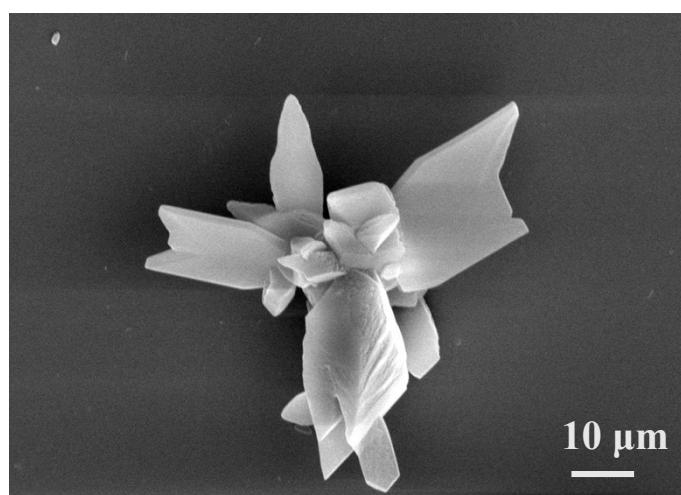


Fig. S11. SEM images of HOF-C-TRZ.

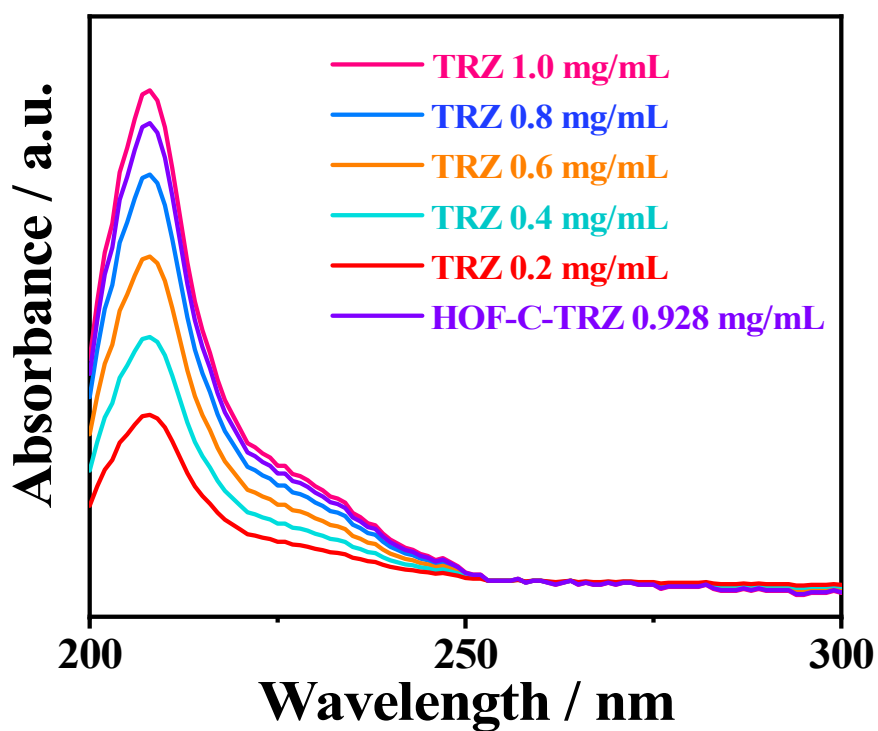


Fig. S12. UV-vis spectra of different concentrations of TRZ solutions before and after the immersion of HOF-C.

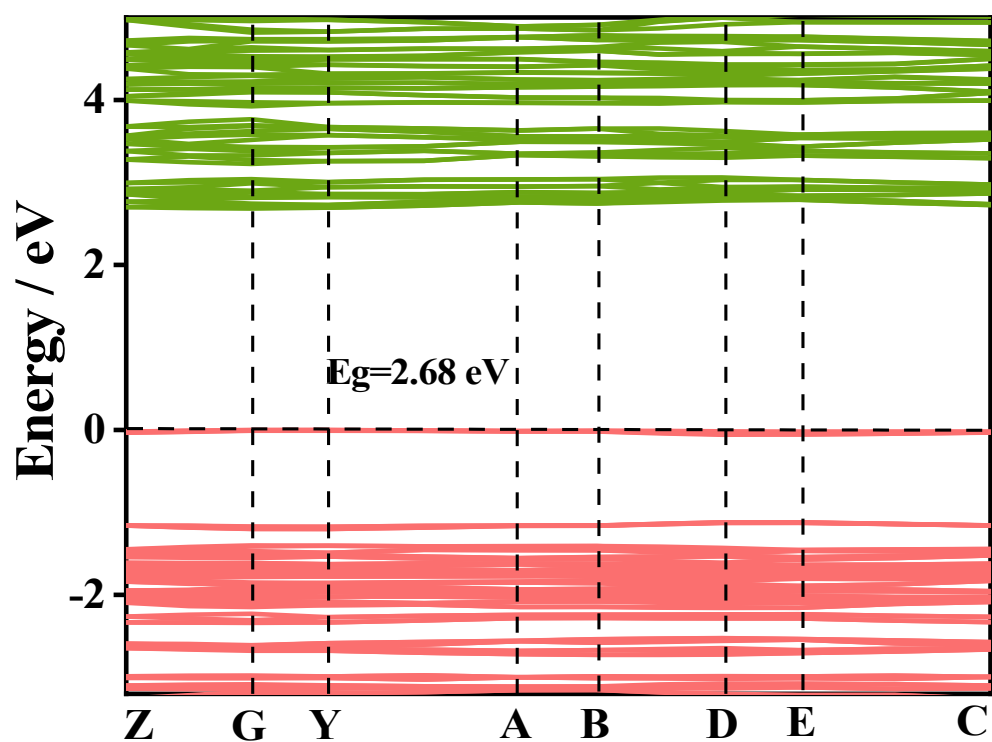


Fig. S13. The electronic band structure of HOF-K.

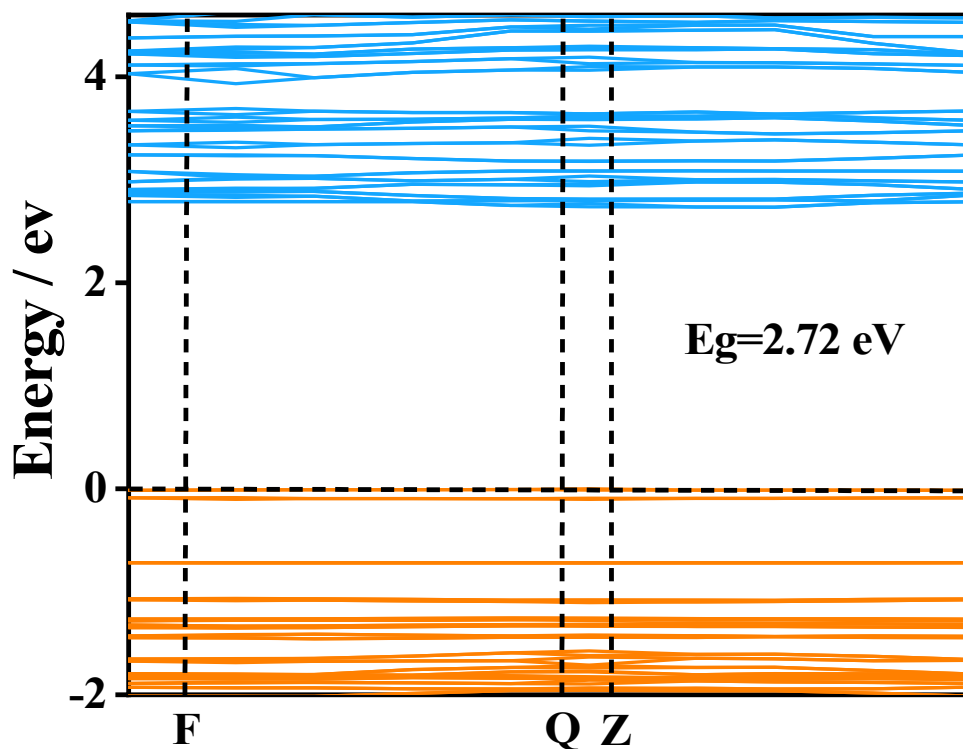


Fig. S14. The electronic band structure of HOF-C.

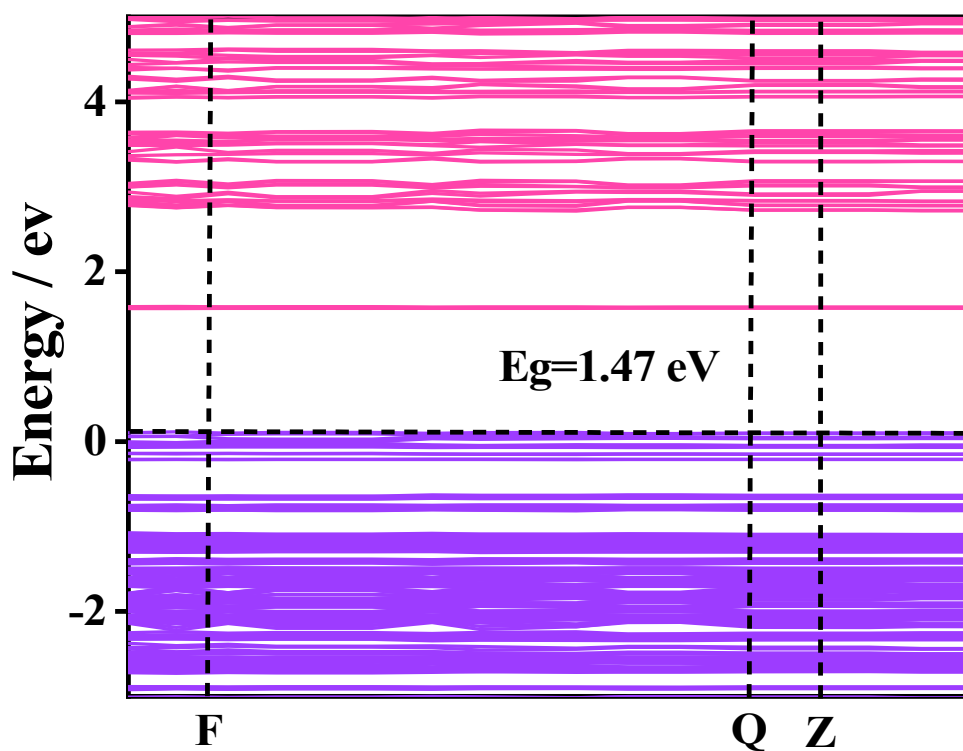


Fig. S15. The electronic band structure of HOF-C-TRZ.

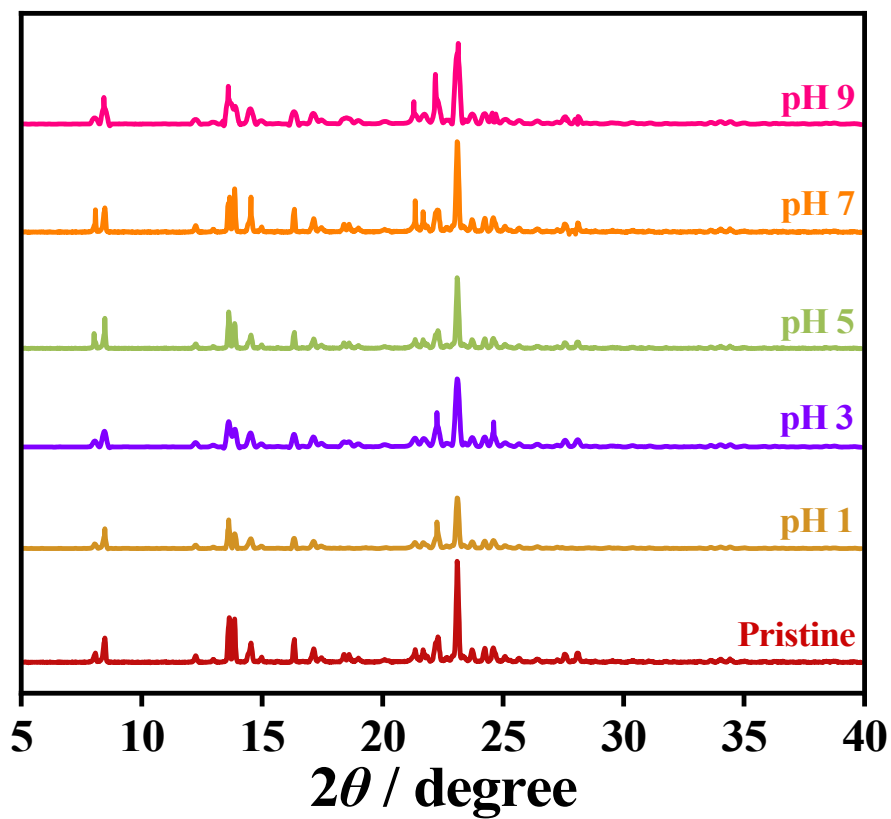


Fig. S16. PXRD patterns of HOF-C-TRZ at different pH values.

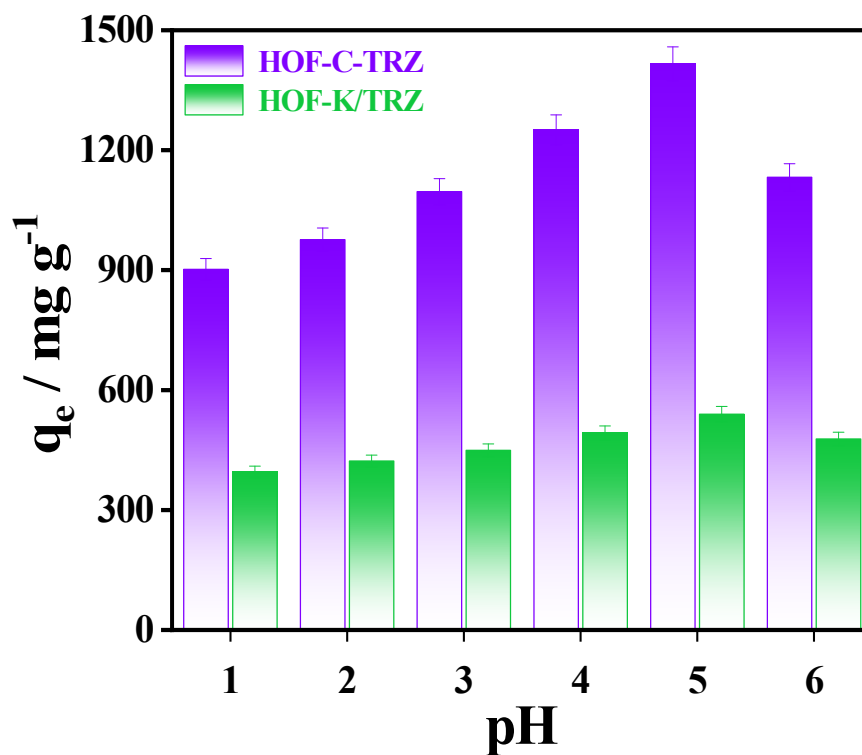


Fig. S17. The uranium recovery capacity of HOF-C and HOF-K with different pH.

Table S3. Comparison of various catalysts for photoreduction of uranium.

Absorbents	Adsorption capacity (mg g^{-1})	Ref.
K-CN-PHI	119.1	6
MIL-125-P@TiO ₂	614.8	7
MOF-76	298	8
CMPAO	251.9	9
Fe@ZIF-8	277.8	10
KC@C-ZnO-X	738.4	11
HOF-C-TRZ	1416	This work

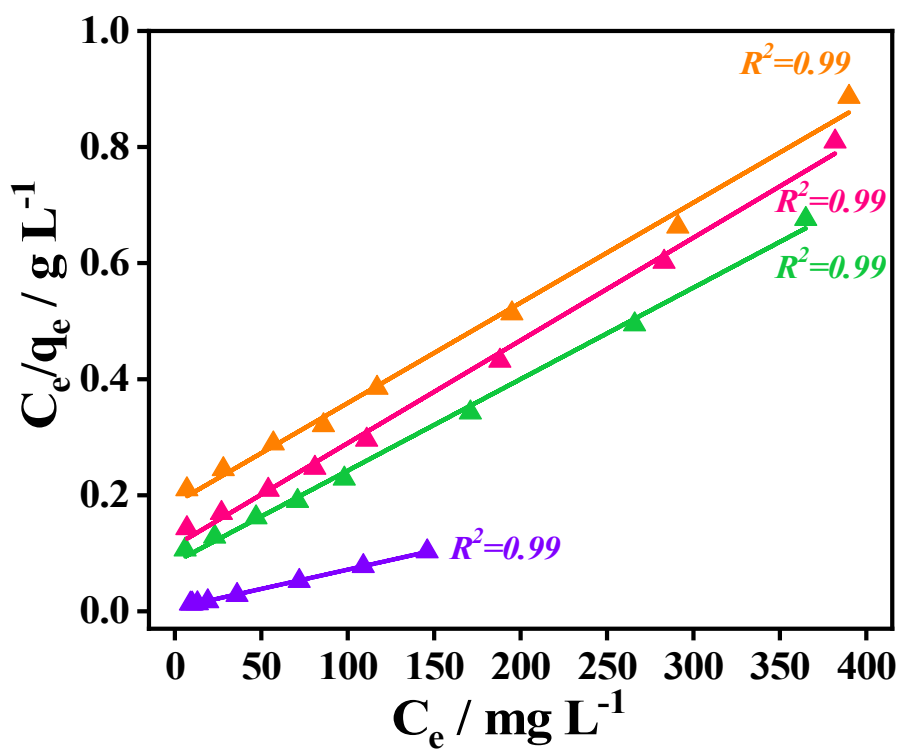


Fig. S18. The linear regression by fitting the equilibrium adsorption data with Langmuir adsorption model.

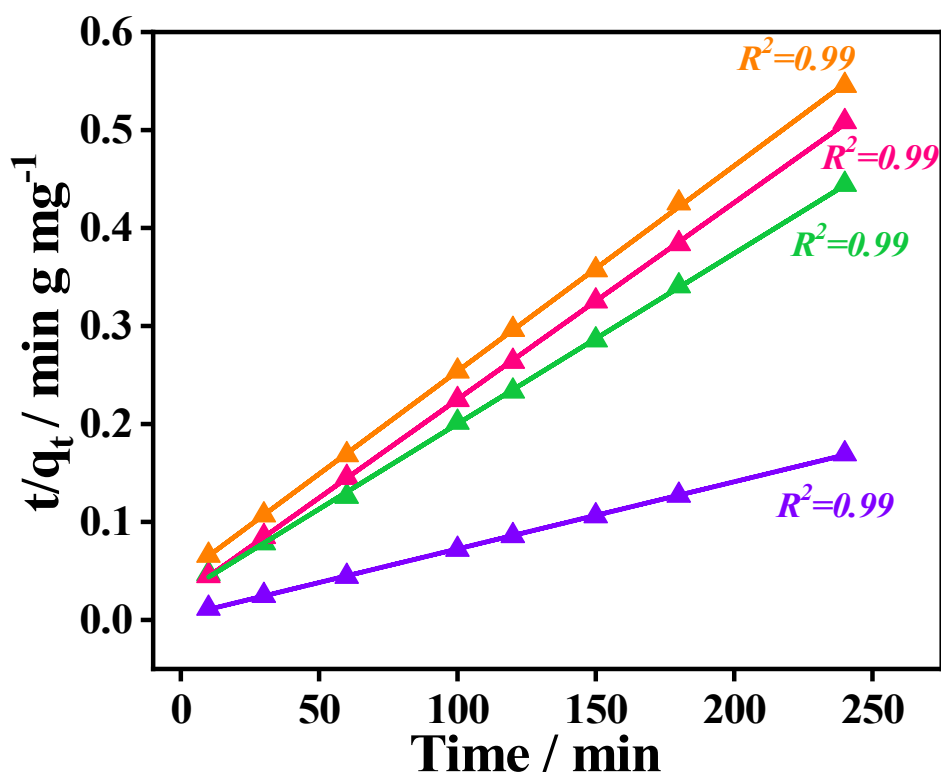


Fig. S19. The pseudo-second-order kinetic curves for the UO_2^{2+} photocatalytic reduction.

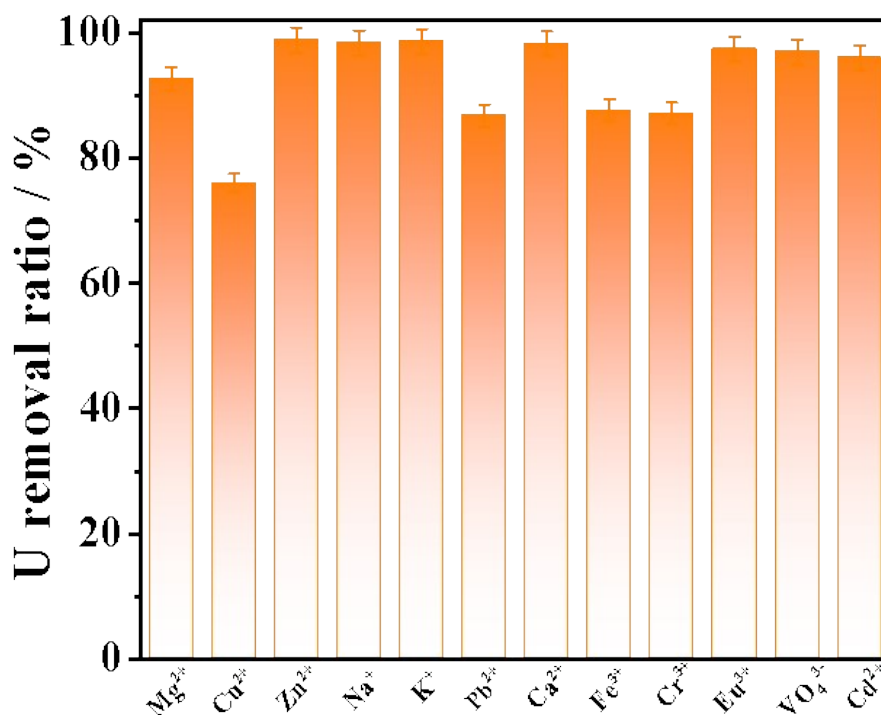


Fig. S20. The selectivity of HOF-C-TRZ to different ions. Error bars represent S.D. n=3 independent experiments.

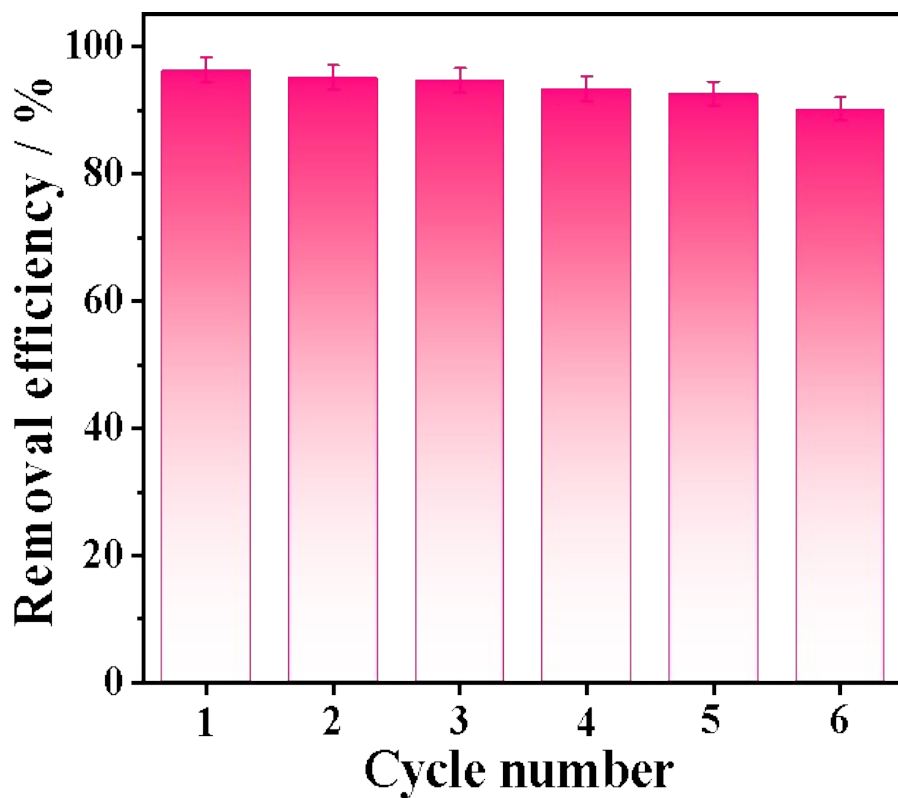


Fig. S21. Cycling performance of UO_2^{2+} photoreduction by HOF-C-TRZ.

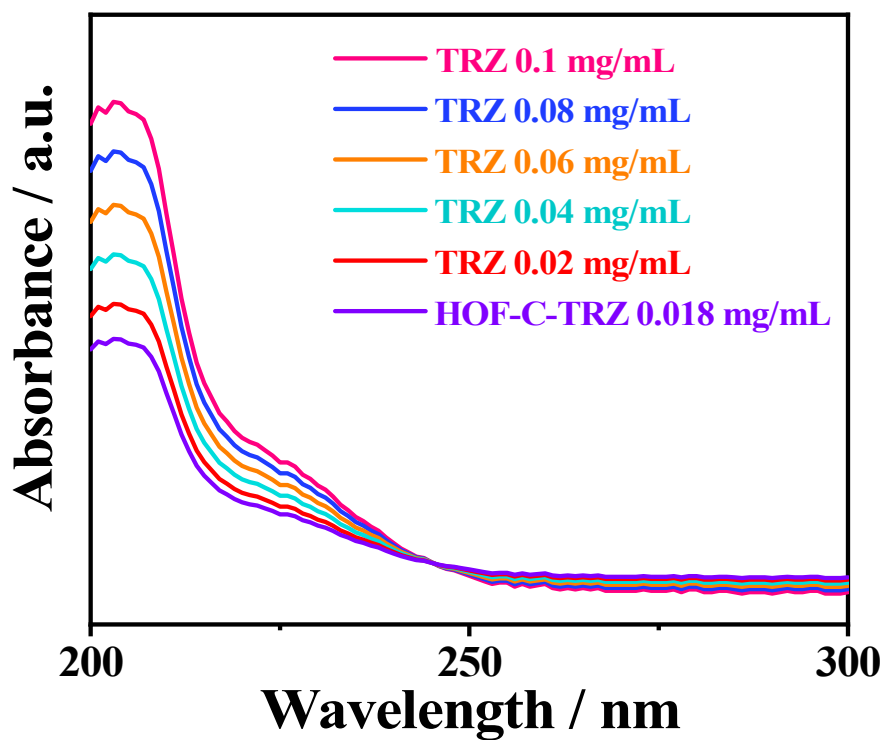


Fig. S22. UV-vis spectrum of 20 mL H_2O after the immersion of 5 mg HOF-C-TRZ.

E_{FB}/V	E_{CB}/V	E_{VB}/V	E_g/eV
-1.32	-1.52	1.21	2.53

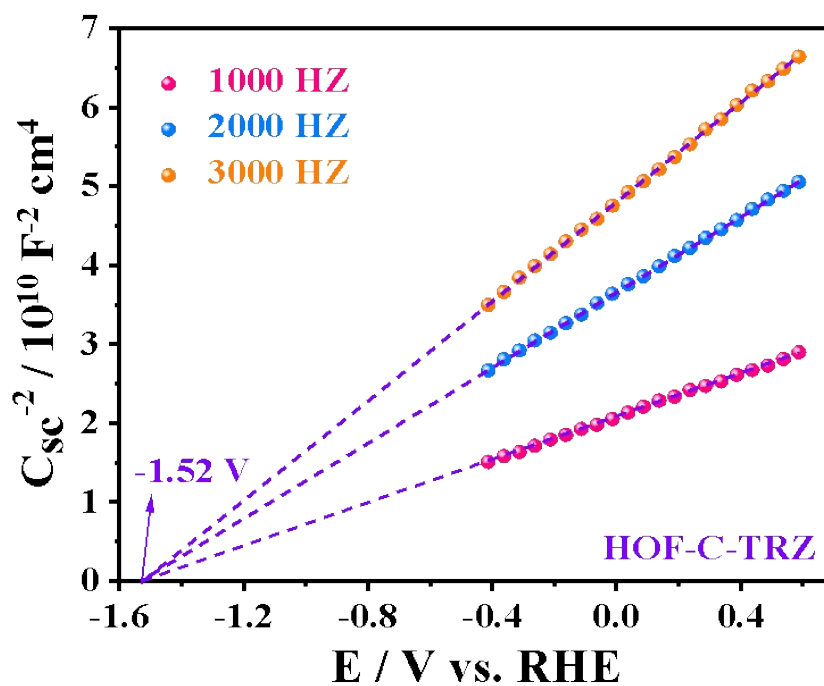


Fig. S23. Mott-Schottky plots of HOF-C-TRZ.

Table S4. Composition and concentration of ions in samples of uranium mine wastewater.

Component of Sample	Concentration
U	0.421 mg L ⁻¹
Cd	0.00023 mg L ⁻¹
Pb	0.00057 mg L ⁻¹
²²⁶ Ra	0.131 Bq L ⁻¹
²¹⁰ Po	0.014 Bq L ⁻¹
²¹⁰ Pb	0.03 Bq L ⁻¹

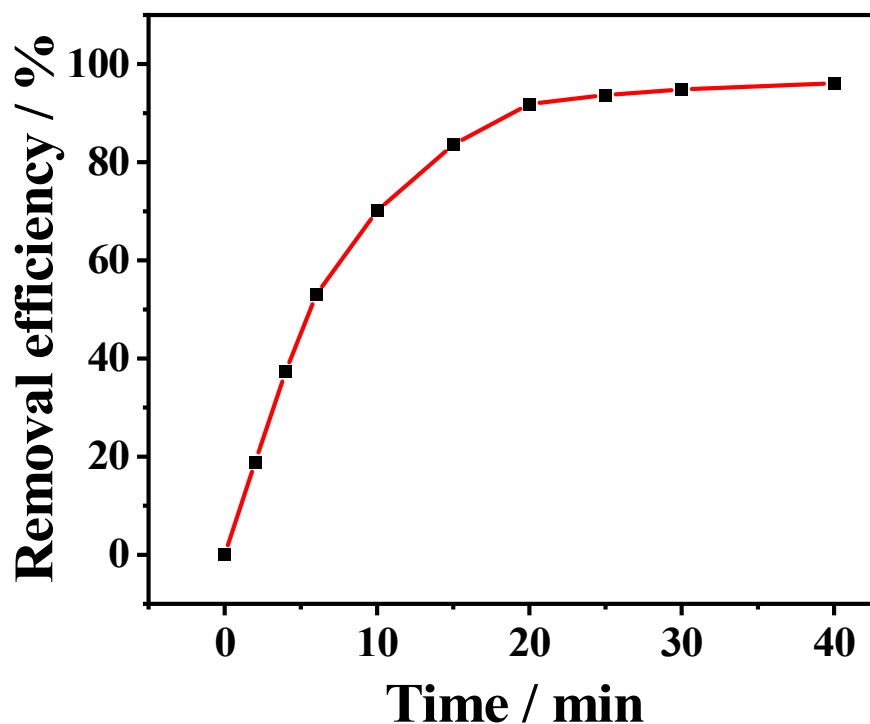


Fig. S24. Adsorption kinetics of UO_2^{2+} by HOF-C-TRZ in real uranium mine wastewater.

4. Supplementary References.

1. G. M, *Acta Cryst. Sect.*, 2015, **71**, 3-8.
2. O. V. Dolomanov, L. J. Bourhis, R. J. Gildea, J. A. K. Howard, H. Puschmann, *J. Appl. Cryst.*, 2009, **42**, 339-341.
3. W.-R. Cui, C.-R. Zhang, R.-H. Xu, X.-R. Chen, W. Jiang, Y.-J. Li, R.-P. Liang, L. Zhang, J.-D. Qiu, *Appl. Catal. B: Environ.*, 2021, **294**, 120250.
4. J. L. Wu, K. Tian, J. L. Wang, *Prog. Nucl. Energy.*, 2018, **106**, 79-86.
5. W.-R. Cui, C.-R. Zhang, W. Jiang, F.-F. Li, R.-P. Liang, J. Liu, J.-D. Qiu, *Nat. Commun.*, 2020, **11**, 436.
6. J. J. Wang, P. Li, Y. Wang, Z. Y. Liu, D. Q. Wang, J. J. Liang, Q. H. Fan, *Adv. Sci.*, 2023, **10**, 2205542.

-
7. C. Xu, W. Zhang, Y. T. Chen, G. Z. Hu, R. Liu, Z. Han, *ChemistrySelect.*, 2019, **4**, 12801-12806.
 8. W. T. Yang, Z.-Q. Bai, W.-Q. Shi, L.-Y. Yuan, T. Tian, Z.-F. Chai, H. Wang, Z.-M. Sun, *Chem. Commun.*, 2013, **49**, 10415-10417.
 9. M. Y. Xu, T. Wang, P. Gao, L. Zhao, L. Zhou, D. B. Hua, *J. Mater. Chem. A*, 2019, **7**, 11214-11222.
 10. X. M. Zhang, Y. Liu, Y. Jiao, Q. H. Gao, P. Wang, Y. Yang, *Micropor. Mesopor. Mat.*, 2019, **277**, 52-59.
 11. R. X. Wang, H. H. Dong, X. Y. Li, L. Zhou, W. K. Zhu, T. Chen, *Chem. Eng. J.*, 2023, **478**, 147331.